PHOTONICS Research

High efficiency all-dielectric pixelated metasurface for near-infrared full-Stokes polarization detection

CHONG ZHANG,[1,2] JINGPEI HU,[1,2,4] YANGENG DONG,[1,2] AIJUN ZENG,[1,2,5] HUIJIE HUANG,[1,2] AND CHINHUA WANG[3]

[1]Laboratory of Information Optics and Optoelectronic Technology, Shanghai Institute of Optics and Fine Mechanics, Chinese Academy of Sciences, Shanghai 201800, China
[2]Center of Materials Science and Optoelectronics Engineering, University of Chinese Academy of Sciences, Beijing 100049, China
[3]Key Laboratory of Advanced Optical Manufacturing Technologies of Jiangsu Province and Key Laboratory of Modern Optical Technologies of Ministry of Education, Soochow University, Suzhou 215006, China
[4]e-mail: hujingpei@siom.ac.cn
[5]e-mail: aijunzeng@siom.ac.cn

Received 18 November 2020; revised 25 January 2021; accepted 3 February 2021; posted 5 February 2021 (Doc. ID 415342); published 31 March 2021

Pixelated metasurfaces integrating both the functions of linear polarization and circular polarization filters on a single platform can achieve full-Stokes polarization detection. At present, the pixelated full-Stokes metasurfaces mainly face the following problems: low transmission, low circular dichroism (CD) of circular polarization filters, and high requirements in fabrication and integration. Herein, we propose high performance ultracompact all-dielectric pixelated full-Stokes metasurfaces in the near-infrared band based on silicon-on-insulator, which is compatible with the available semiconductor industry technologies. Circular polarization filters with high CD are achieved by using simple two-dimensional chiral structures, which can be easily integrated with the linear polarization filters on a single chip. In addition, the dielectric materials have higher transmission than metal materials with intrinsic absorption. We experimentally demonstrated the circular polarization filter with maximum CD up to 70% at a wavelength of 1.6 μm and average transmission efficiency above 80% from 1.48 μm to 1.6 μm. Therefore, our design is highly desirable for many applications, such as target detection, clinical diagnosis, and polarimetric imaging and sensing.

https://doi.org/10.1364/PRJ.415342

1. INTRODUCTION

Polarization, the same as intensity, wavelength, and phase, is an important characteristic of light. Conventional imaging techniques only capture the intensity and spectral information of light, but ignore the polarization information in the scene. Deeper information about the materials, like surface shape, roughness, optical activity of the materials, and chemical properties, can be obtained from the polarization state of light. Polarimetric imaging techniques can obtain polarization state of light over a scene of interest, which play an important role in many applications, such as astronomy [1], chemical analysis [2], remote sensing [3–5], and biomedical diagnosis [6,7].

Conventional polarimetry approaches rely on mechanically rotating polarizers [8] and retardation wave plates [9] several times, which takes long acquisition time and is unavailable for dynamic events. Moreover, the optical components are bulky and do not conform to the current trends of integration and miniaturization [10,11]. Pixelated metasurfaces [12–14] combined with a charge coupled device (CCD) to obtain real-time polarization imaging can overcome the shortcomings of the conventionally mechanical rotating polarization imaging, which can acquire the polarization state of incident light at one time. These methods are more compact and less expensive, require less convoluted optic systems, and are the primary development directions of polarization imaging in the future. As we all know, the polarization state of light is usually described by Stokes vector $\boldsymbol{S}$, comprised by four components (S_0, S_1, S_2, S_3), which are related to the intensities of linearly and circularly polarized parts of the incident light. Most of the pixelated metasurfaces are composed of nanowire-grid polarization filters [15–17] in different directions, which work on linearly polarized light but not circularly polarized light, so only part of the Stokes vector (S_0, S_1, S_2) can be detected through it.

Over the past years, metasurfaces with great design flexibility and ultracompact form factors provide a great choice for circularly polarized light detection and have attracted lots of attention [18–25]. Among these designs, three-dimensional (3D) chiral plasmonic metasurfaces can acquire a higher

circular polarization (CP) extinction ratio than the planar chiral plasmonic metasurfaces. However, these 3D metasurfaces are difficult to integrate with nanowire-grid polarization filters on a single layer. To overcome this difficulty, double-layer planar plasmonic metasurfaces consisting of waveplates and polarizers as CP filters were designed and fabricated, while the transmission of the filters is extremely low [26,27], and their fabrication technology is complex [26–28]. Compared with plasmonic metasurfaces, all-dielectric structures avoid absorption losses and have compatibility with available semiconductor industry technologies. Recently, all-dielectric metasurfaces composed of multiple microscale scatterers, which split and focus light in four or six different polarization bases, were reported with high transmission to realize full-Stokes detection of incident light [11,29–31]. However, these kinds of metasurfaces can only be designed for a single wavelength, and the crosstalk between different polarization states interferes with the measurement results when the super-pixel becomes smaller.

Here, we propose and experimentally demonstrate ultracompact high performance all-dielectric pixelated full-Stokes metasurfaces for the near-infrared wavelength. Each pixel consists of linear polarizers in three directions and one circular polarizer with single-layer planar structures. All of these polarizers can be integrated on a silicon-on-insulator (SOI) chip, which is compatible with mature semiconductor industry technologies nowadays. The proposed all-dielectric pixelated full-Stokes metasurfaces are more advantageous due to their ultracompactness, high extinction ratio, high transmission efficiencies, and broad operating wavelength, which can meet the measurement requirements of many applications.

2. PIXELATED METASURFACE DESIGN

The polarization measurement device is shown in Fig. 1(a), which includes the all-dielectric metasurface and the CCD array. The polarization filters in the metasurface and the polarization components of their corresponding exit light are shown with different colors in Fig. 1(a); the colors are not related to the material and wavelength. In fact, the CCD array is directly attached to the metasurface. In order to visualize the splitting light function of the metasurface, the distance between the metasurface and the CCD array is enlarged in the figure. The key element of this device is the all-dielectric metasurface, which contributes to the polarization splitting of incident light. The metasurface is composed of multiple pixels, and each pixel has four spatially distributed polarization filters (F_0 to F_3), as shown in Fig. 1(b). The linear polarization (LP) filters (F_0, F_1, F_2) are nanowire gratings oriented in three different directions to transmit linearly polarized light, whose directions of electric field vectors are oriented at 0°, 90°, 45° with respect to the x axis, respectively. As shown in Fig. 1(d), the LP filters transmit the TM polarized light with the electric field direction perpendicular to the grating grooves, while blocking the transmission of TE polarized light with the electric field direction parallel to the grating grooves. The F_3, a CP filter shown in Fig. 1(c), with simple Z-shaped planar patterns, transmits

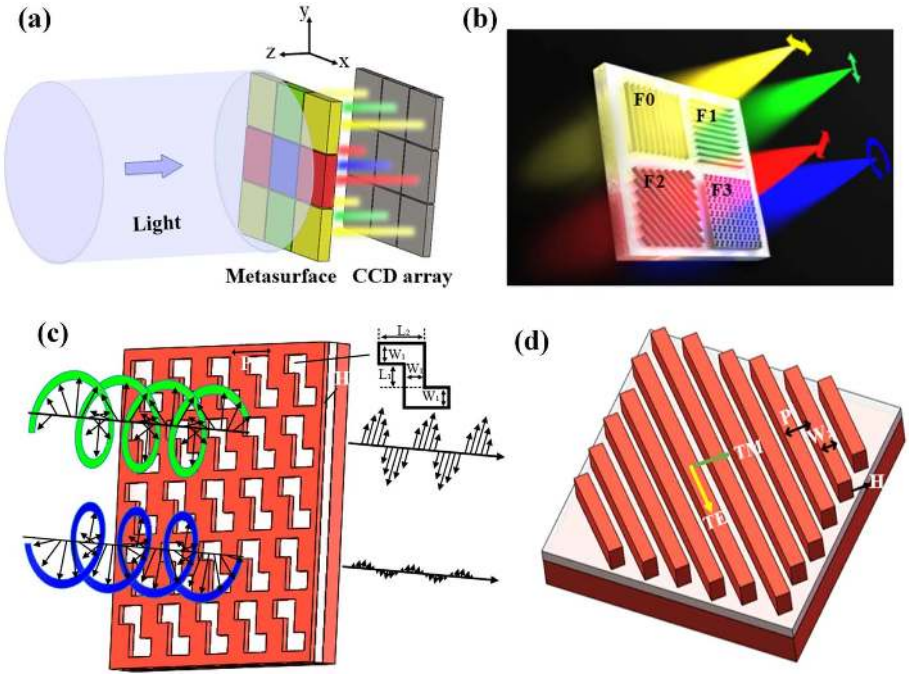

Fig. 1. Schematic of setup for near-infrared full-Stokes detection. (a) Polarization measurement device with the metasurface and the CCD array. Each pixel of the metasurface is composed of four different polarization filters. (b) Three-dimensional schematic of the pixel unit with four spatially distributed polarization filters. The colors are used only for distinguishment of the image and bear no wavelength information. (F_0, F_1, F_2) and F_3 represent LP and CP filters, respectively. (c) CP filter with the Z-shaped pattern, which transmits right-circularly polarized light (green) and blocks left-circularly polarized light (blue). (d) LP filter consists of the nanowire grid grating, which transmits (blocks) TM (TE) polarized light with the electric field vector perpendicular (parallel) to the grating grooves.

right-handed circularly polarized (RCP) light and blocks left-handed circularly polarized (LCP) light. The intensity of different polarization components in incident light that will pass through our polarization filters can be described as $I_{0°}$, $I_{90°}$, $I_{45°}$, and I_R, respectively. All of the pixels can be integrated on a single SOI wafer, which is composed of three parts: the silicon bottom substrate, insulating thin silicon dioxide middle layer, and monocrystalline silicon top layer, which is the device layer. The devices based on the SOI wafer have the advantages of high integrity, low power consumption, and high temperature resistance and are increasingly favored by the industry. When incident light is perpendicular across the metasurface, the polarization filters at different positions will filter the incident light accordingly, and then the CCD array right behind the metasurface can detect the intensities of different polarization components. Then, by further analyzing the polarization components, full-Stokes parameters can be retrieved. The derivation process is shown in the following.

As we know, the full-Stokes vectors $\boldsymbol{S}$ have four parameters S_0, S_1, S_2, S_3 and are defined as

$$S_0 = I_{0°} + I_{90°} = I_{45°} + I_{135°} = I_R + I_L, \tag{1}$$

$$S_1 = I_{0°} - I_{90°}, \tag{2}$$

$$S_2 = I_{45°} - I_{135°}, \tag{3}$$

$$S_3 = I_R - I_L, \tag{4}$$

where $I_{0°}$, $I_{90°}$, $I_{45°}$, and $I_{135°}$ represent the intensities of LP components along 0°, 90°, 45°, and 135° with respect to the x axis. I_R and I_L are the intensity of RCP and LCP light, respectively. The above parameters ($I_{0°}$, $I_{90°}$, $I_{45°}$, I_R) are theoretical values that cannot be measured accurately due to imperfections of the filters in the metasurface. In this condition, the equation $I_{45°} + I_{90°} = I_{45°} + I_{135°} = I_R + I_L$ also cannot be used. Therefore, in this work, we have considered the imperfections of actual filters in the metasurface and ignorable absorption of dielectric materials [32] in this operation wavelength range. The relationships of intensities between the measured polarization components and polarization components in the incident light are defined as follows:

$$I'_{0°} = t_{\mathrm{TM}} I_{0°} + t_{\mathrm{TE}} I_{90°}, \tag{5}$$

$$I'_{90°} = t_{\mathrm{TM}} I_{90°} + t_{\mathrm{TE}} I_{0°}, \tag{6}$$

$$I'_{45°} = t_{\mathrm{TM}} I_{45°} + t_{\mathrm{TE}} I_{135°}, \tag{7}$$

$$I'_R = t_R I_R + t_L I_L, \tag{8}$$

where ($I'_{0°}$, $I'_{90°}$, $I'_{45°}$, I'_R) represent actual measured intensities of incident light after passing through four pixel units, respectively. t_{TM} and t_{TE} are the transmission coefficients of LP filters for TM and TE light, respectively. t_R and t_L are the transmission coefficients of CP filters for RCP and LCP light, respectively. Combining the transmission coefficients (t_{TM}, t_{TE}, t_R, t_L) of the pixelated metasurface with measured intensities of ($I'_{0°}$, $I'_{90°}$, $I'_{45°}$, I'_R), the $I_{0°}$ and $I_{90°}$ can be obtained with Eqs. (5) and (6). Then, combining Eq. (1) with Eqs. (7) and (8), $I_{45°}$, $I_{135°}$, I_R, and I_L can be acquired. Finally, the full-Stokes vector $\boldsymbol{S}$ of incident light can be calculated. With this method of calculation, the measurement errors are effectively reduced compared to other literatures [27,28].

In this section, the finite difference time domain (FDTD) method (Lumerical FDTD solutions, Canada) is adopted to design and optimize pixel units of the metasurface in the near-infrared wavelength range from 1.4 μm to 1.65 μm, which is an atmosphere window for information communication [33]. In order for the LP and CP filters to be easily integrated on a single chip, the design should ensure that all of the filters have equal etching depth. On that basis, it also needs to assure the polarization performance of the metasurface, such as transmission, extinction ratio, and circular dichroism (CD), which tremendously increases the difficulty of the design. To simplify the design of the metasurface, the polarization effects of LP and CP filters are simulated separately. First, the CP filter with the Z-shaped pattern hole array on the SOI wafer is designed and optimized, as shown in Fig. 1(c), in which W_1, P, L_1, and L_2 stand for the width of the slot, period of the structure, vertical distance of the horizontal slot, and length of the horizontal slot. The structure with the Z-shaped pattern cannot overlap with its mirror image; therefore, the CP filter is a chiral structure. The chiral structure has different transmission to RCP and LCP light, resulting in CD [32,34]. In the simulation, the parameters of SOI are set as silicon bottom substrate of 675 μm, silicon dioxide middle layer of 3 μm, and silicon top layer of 0.22 μm. The periodic boundary conditions are used along the x and y directions owing to the periodicity of the structures, while perfectly matched layers (PMLs) along the z direction are used. The dielectric properties of Si and SiO_2 are adopted by Palik [35]. Two types of circularly polarized light, RCP and LCP light, are assumed to be incident from the substrate along the z direction. The default accuracy of the FDTD solutions software is adopted for the simulation region. Figure 2(a) shows the transmission spectra of circularly polarized light at the optimized parameters as $W_1 = 0.32$ μm, $L_1 = 0.22$ μm, $L_2 = 0.48$ μm, $H = 0.22$ μm, and $P = 0.98$ μm. It can be seen that the average transmission of the RCP light is almost close to 85%, which cannot be achieved by a metal metasurface. To show the physical mechanism of CD, Figs. 2(c) and 2(d) plot the cross section of the electric field at $H = 0.2$ μm when the RCP light and LCP light pass through the Z-shaped slot at a response wavelength of 1.6 μm, respectively. For LCP light, as shown in Fig. 2(d), a strong local resonant electric field can be seen between the Z-shaped air slots and the Si ridged core, due to strong coupling interaction when the handedness of LCP light is the same as chiral structure. While the handedness of RCP light is opposite LCP light, there is no such coupling effect in the structure, so the RCP light can pass through the structure, as witnessed in Fig. 2(c). The transmission difference between RCP and LCP light is very large at the response wavelength. As shown in Fig. 2(b), at a wavelength of 1.6 μm, the CD can be as high as 90%. The CD can reach more than 50% in the wavelength range from 1.48 μm to 1.54 μm and 1.59 μm to 1.61 μm, which satisfies the dichroism requirement for most applications.

In the following, on the basis of the same etching depth and period of the CP filter, the duty ratio of grating LP filters is optimized to make it have good polarization performance in

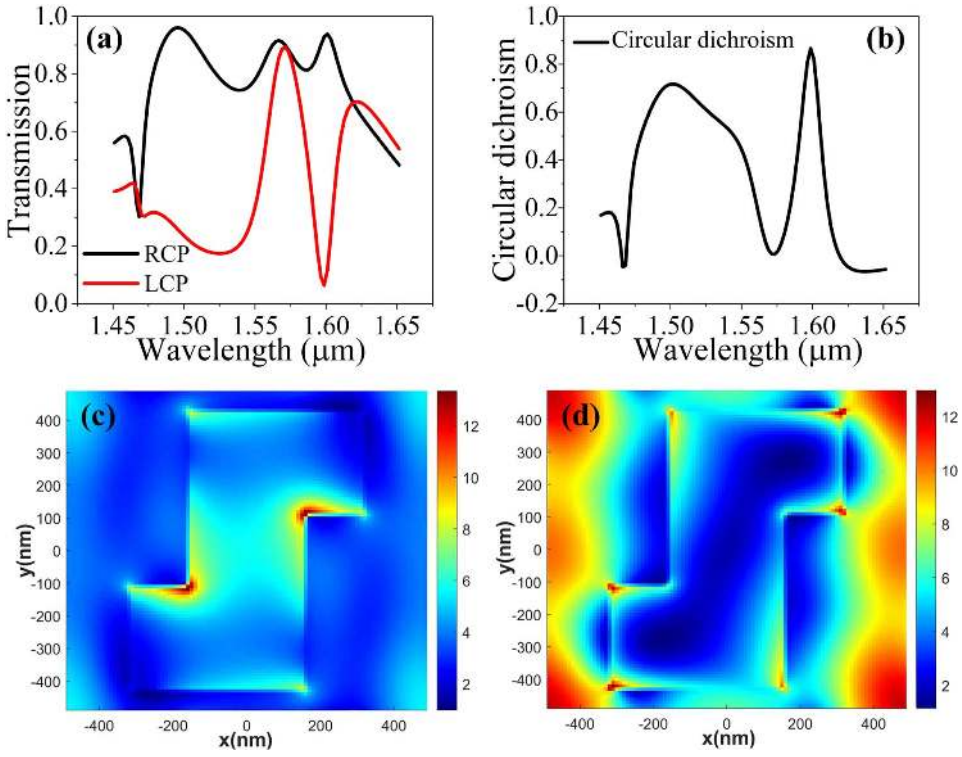

Fig. 2. Simulation performances of the CP filters. (a) Transmission spectra of the CP filter for RCP (black) and LCP (red) light as the parameters of the Z-shaped pattern are as follows: $W_1 = 0.32$ μm, $L_1 = 0.22$ μm, $L_2 = 0.48$ μm, $H = 0.22$ μm, and $P = 0.98$ μm. (b) The corresponding CD of the CP filter. The electric field cross section diagram at $H = 0.2$ μm for (c) RCP light and (d) LCP light at the wavelength of 1.6 μm.

the operating band of CP filters. The setting of simulation conditions, material properties, and SOI parameters are the same as that of the CP filter. With the optimized width of the ridge $W_2 = 0.34$ μm of the grating [as shown in Fig. 1(d)], the average transmission of TM polarized light is above 80% in the operation wavelength range from 1.45 μm to 1.6 μm, and the maximum transmission can even reach 90% at the wavelength of 1.52 μm, as shown in Fig. 3(a). The corresponding extinction ratio $[10 \times \log(t_{TM}/t_{TE})]$ of the LP filters is more than 20 dB, and the maximum can reach 70 dB at the 1.54 μm wavelength, which can be seen in Fig. 3(b). To further explore the physical mechanism of the high extinction ratio at the 1.54 μm wavelength, the electric field cross section diagrams of the dielectric grating filter for TM and TE polarized light are shown in Figs. 3(c) and 3(d), respectively. As we can see in Fig. 3(d), most of the electric field energy of TM polarized light passes through the grating region, while almost all of the electric field energy of TE polarized light is confined to the grating and substrate region [36]. Therefore, the LP filters can transmit TM light and filter out TE light.

3. FABRICATION AND EXPERIMENTAL RESULTS

In the fabrication, both 3D and double-layer chiral metasurfaces face the challenge of integrating with the polarization nanowire gratings. In our design, the CP and LP filters not only adopt single-layer structures but also hold equal etching depths and periods, which can enormously simplify and reduce the difficulties in the fabrication. First, we spin coat a PMMA of about 100 nm thickness onto a cleaned SOI substrate. Under the optimized parameters of metasurfaces, the nanogratings and Z-shaped plane structures were patterned on the substrate with electron beam lithography (EBL) (Pionner@Entire 3, Raith). The substrate was fixed to the platform with conductive adhesive tape that enhances the conductivity of the substrate. After development of the resist, the inductively coupled plasma etching technique (C_4F_8:SF_6:O_2 = 80:60:5 sccm, standard cubic centimeters per minute) with an etching rate of 10:1 was applied to etch the sample. It should be noted that the etching rate of the substrate should be firstly measured using a dummy wafer, and then the etching depth can be precisely controlled during etching to certify the polarization performance of the metasurface. Figure 4(a) shows a scanning electron microscope (SEM) image of the fabricated full-Stokes polarimeter metasurface, in which each pixel has a size of 14 μm × 14 μm, and there is 1 μm spacing [37] between pixels to prevent interference of cross talk between adjacent pixels. Figures 4(b) and 4(c) show the enlarged SEM images of LP and CP filters of the fabricated metasurface, respectively. It is shown that the parameters of the fabricated structures are consistent with their theoretical ones.

To conveniently characterize the performance of the metasurface, the LP and CP filters with the size of 1 mm × 1 mm were fabricated by using the same fabrication technology parameters, respectively. The measurement setup of the CP filter is illustrated in Fig. 5(a). The wide spectrum supercontinuum laser source (Fianium, SC450) was firstly divided into

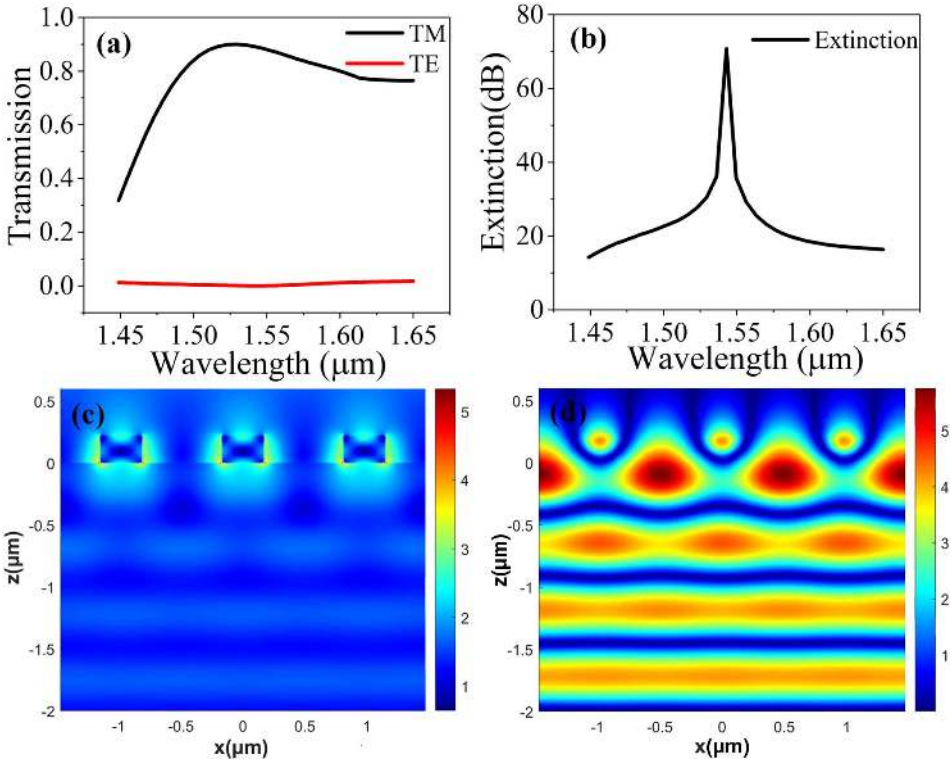

Fig. 3. Simulation performances of the LP filters. (a) Transmission spectra of the LP filter for TM (black) and TE (red) light as the parameters of nanowire gratings are as follows: $W_2 = 0.32$ μm, $H = 0.22$ μm, and $P = 0.98$ μm. (b) The corresponding extinction ratio of the LP filter. The electric field cross section diagram of the dielectric grating filter for (c) TM light and (d) TE light at the response wavelength of 1.54 μm.

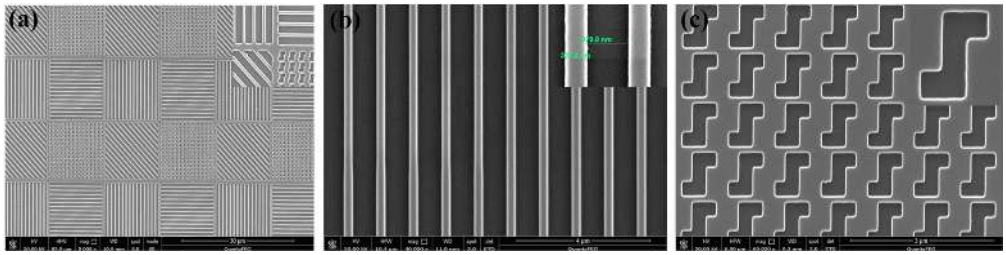

Fig. 4. Scanning electron microscope (SEM) image. (a) SEM image of the fabricated devices. (b) Enlarged SEM image of the LP filters with nanowire gratings. (c) Enlarged SEM image of the CP filters with the Z-shaped pattern.

monochromatic light by a monochromator. Then, the monochromatic light formed polarized light through the collimation system and infrared linear polarizer in turn. The polarized monochromatic light passing through a quarter waveplate (QWP) (Alphalas GmbH, PO-TWP-L4-12-UVIR) produced circularly polarized light. By adjusting the angle of the linear polarizer and the fast axis of the QWP, the different handedness of circularly polarized light can be controlled. The light was then focused onto the sample by an objective. Finally, the light intensity was detected by a free space polarization detector (Thorlabs, PAX10IR3-T). The measured transmission spectra of LCP and RCP light and corresponding CD are shown in Figs. 5(b) and 5(c), respectively. Obviously, the measurement results are consistent with the theoretical results in Figs. 2(a) and 2(b). The measured CD is more than 50% in the wavelength range from 1.49 μm to 1.54 μm, and the maximum can reach 70% at 1.6 μm.

After removing the QWP and replacing the CP filter with the LP filter, the performance of the LP filter can be directly tested. The measured transmission spectra for TE and TM polarized light of the LP filter are shown in Fig. 5(d). The average transmission for TM polarized light is measured at around 75% in the wavelength range of 1.47 μm to 1.6 μm. The corresponding extinction ratio is shown in Fig. 5(e). It is indicated that the extinction ratio is greater than 20 dB in the wavelength range from 1.49 μm to 1.6 μm, and the maximum can reach 34 dB at 1.52 μm. Compared with the theoretical results, the peak of the corresponding extinction ratio shows a slight blue

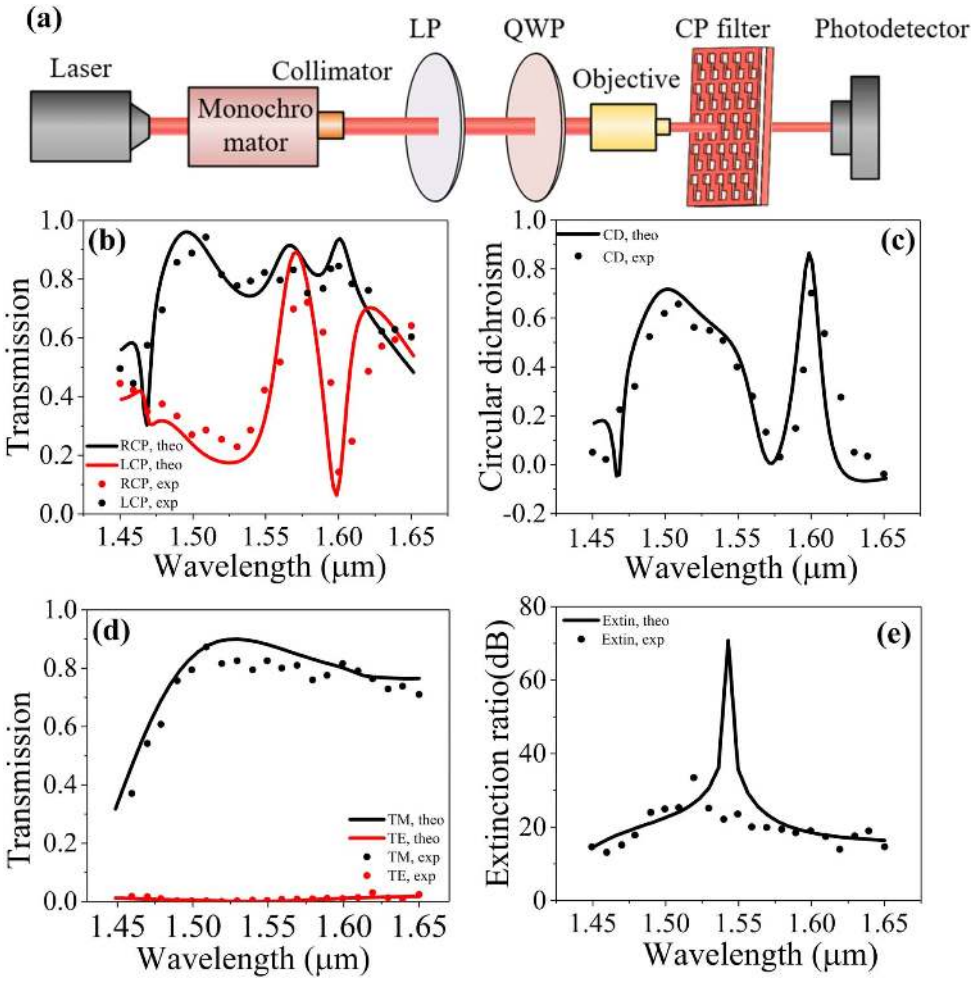

Fig. 5. Experimental setup and measurement results of the LP and CP filters. (a) Schematic of the measurement setup for CP filter characterization. (b) Transmission spectra of RCP and LCP light and (c) corresponding CD of the CP filter. (d) Transmission spectra of TM and TE polarized light and (e) corresponding extinction ratio of the LP filter.

shift and declines significantly. The slight blue shift may be caused by over etching in the fabrication, and the reason for the decline of the extinction ratio is associated with the sensitivity of the photodetector. When the transmission of TE polarized light is lower than the lowest sensitivity of the detector, the optical signal can be drowned by noise, which significantly reduces the maximum extinction ratio. From these experiment results of the LP and CP filters, the metasurface is competent to detect the full-Stokes vector of incident light in the wavelength ranges from 1.49 μm to 1.54 μm and from 1.59 μm to 1.61 μm.

4. CONCLUSION

In conclusion, we designed and fabricated a pixelated all-dielectric metasurface based on the SOI substrate for full-Stokes vector detection in the near-infrared band. The pixel unit of the metasurface is composed of four different polarization filters including LP and CP filters. With equal etching depths, periods, and simple structure, the CP and LP filters are easily integrated on the same chip, which is compatible with conventional semiconductor industry technologies. We experimentally demonstrated the performance of the metasurface by testing the polarization effects of different filters, respectively. With a simple two-dimensional etching pattern, the CP filters can well distinguish the handedness of circularly polarized light with CD as high as 70% at 1.6 μm and average transmission efficiency of more than 80% from 1.48 μm to 1.6 μm. By optimizing the parameters of the grating in the same operation wavelength band, the LP filters have a great polarization effect for linearly polarized light. Comparably, our device has great potential for near-infrared polarimeters and on-chip polarimetric imaging systems, which are desirable for material characterization, medical diagnosis, biomedical imaging, and molecular spectroscopy.

Funding. International Science and Technology Cooperation Programme (20500711300); National Natural Science Foundation of China (61805264); Shanghai Sailing Program (18YF1426500); University Scientific Research Foundation of Jiangsu Province (KJS1713).

Disclosures. The authors declare no conflicts of interest.

REFERENCES

1. J. B. Breckinridge and B. R. Oppenheimer, "Polarization effects in reflecting coronagraphs for white-light applications in astronomy," Astrophys. J. **600**, 1091–1098 (2004).
2. L. A. Nafie and T. B. Freedman, "Vibrational circular dichroism: an incisive tool for stereochemical applications," Enantiomer **3**, 283–297 (1998).
3. N. J. Pust and J. A. Shaw, "Digital all-sky polarization imaging of partly cloudy skies," Appl. Opt. **47**, H190–H198 (2008).
4. J. S. Tyo, D. H. Goldstein, D. B. Chenault, and J. A. Shaw, "Polarization in remote sensing-introduction," Appl. Opt. **45**, 5451–5452 (2006).
5. J. S. Tyo, D. L. Goldstein, D. B. Chenault, and J. A. Shaw, "Review of passive imaging polarimetry for remote sensing applications," Appl. Opt. **45**, 5453–5469 (2006).
6. M. Dubreuil, P. Babilotte, L. Martin, D. Sevrain, S. Rivet, Y. L. Grand, G. L. Brun, B. Turlin, and B. L. Jeune, "Mueller matrix polarimetry for improved liver fibrosis diagnosis," Opt. Lett. **37**, 1061–1063 (2012).
7. R. Patel, A. Khan, R. Quinlan, and A. N. Yaroslavsky, "Polarization sensitive multimodal imaging for detecting breast cancer," Cancer Res. **74**, 4685–4693 (2014).
8. H. G. Berry, G. Gabrielse, and A. E. Livingston, "Measurement of the Stokes parameters of light," Appl. Opt. **16**, 3200–3205 (1977).
9. R. M. A. Azzam and N. M. Bashara, *Ellipsometry and Polarized Light* (Elsevier, 1977).
10. K. P. Gurton, A. J. Yuffa, and G. W. Videen, "Enhanced facial recognition for thermal imagery using polarimetric imaging," Opt. Lett. **39**, 3857–3859 (2014).
11. S. Wei, Z. Yang, and M. Zhao, "Design of ultracompact polarimeters based on dielectric metasurfaces," Opt. Lett. **42**, 1580–1583 (2017).
12. Z. Zhang, F. Dong, K. Qian, Q. Zhang, W. Chu, Y. Zhang, X. Ma, and X. Wu, "Real-time phase measurement of optical vortices based on pixelated micropolarizer array," Opt. Express **23**, 20521–20528 (2015).
13. X. Ma, F. Dong, Z. Zhang, Y. Su, T. Xu, Z. Jiang, S. Wu, Q. Zhang, W. Chu, and X. Wu, "Pixelated-polarization-camera-based polarimetry system for wide real-time optical rotation measurement," Sens. Actuators B **283**, 857–864 (2019).
14. J. Guo and D. Brady, "Fabrication of thin-film micropolarizer arrays for visible imaging polarimetry," Appl. Opt. **39**, 1486–1492 (2000).
15. V. Gruev, A. Ortu, N. Lazarus, J. Van der Spiegel, and N. Engheta, "Fabrication of a dual-tier thin film micropolarization array," Opt. Express **15**, 4994–5007 (2007).
16. V. Gruev, R. Perkins, and T. York, "CCD polarization imaging sensor with aluminum nanowire optical filters," Opt. Express **18**, 19087–19094 (2010).
17. G. P. Nordin, J. T. Meier, P. C. Deguzman, and M. W. Jones, "Micropolarizer array for infrared imaging polarimetry," J. Opt. Soc. Am. A **16**, 1168–1174 (1999).
18. Z. Yang, M. Zhao, P. Lu, and Y. Lu, "Ultrabroadband optical circular polarizers consisting of double-helical nanowire structures," Opt. Lett. **35**, 2588–2590 (2010).
19. B. Frank, X. Yin, M. Schäferling, J. Zhao, S. M. Hein, P. V. Braun, and H. Giessen, "Large-area 3D chiral plasmonic structures," ACS Nano **7**, 6321–6329 (2013).
20. M. Zhang, V. Pacheco-Peña, Y. Yu, W. Chen, N. J. Greybush, A. Stein, N. Engheta, C. B. Murray, and C. R. Kagan, "Nanoimprinted chiral plasmonic substrates with three-dimensional nanostructures," Nano Lett. **18**, 7389–7394 (2018).
21. J. K. Gansel, M. Thiel, M. S. Rill, M. Decker, K. Bade, V. Saile, G. Freymann, S. Linden, and M. Wegener, "Gold helix photonic metamaterial as broadband circular polarizer," Science **325**, 1513–1515 (2009).
22. M. Decker, M. Klein, M. Wegener, and S. Linden, "Circular dichroism of planar chiral magnetic metamaterials," Opt. Lett. **32**, 856–858 (2007).
23. D. Kwon, P. L. Werner, and D. H. Werner, "Optical planar chiral metamaterial designs for strong circular dichroism and polarization rotation," Opt. Express **16**, 11802–11807 (2008).
24. F. Afshinmanesh, J. S. White, W. Cai, and M. L. Brongersma, "Measurement of the polarization state of light using an integrated plasmonic polarimeter," Nanophotonics **1**, 125–129 (2012).
25. W. Ye, X. Yuan, C. Guo, J. Zhang, B. Yang, and S. Zhang, "Large chiroptical effects in planar chiral metamaterials," Phys. Rev. Appl. **7**, 054003 (2017).
26. J. Dong, J. Zhou, T. Koschny, and C. Soukoulis, "Bi-layer cross chiral structure with strong optical activity and negative refractive index," Opt. Express **17**, 14172–14179 (2009).
27. J. Bai, C. Wang, X. Chen, A. Basiri, C. Wang, and Y. Yao, "Chip-integrated plasmonic flat optics for mid-infrared full-Stokes polarization detection," Photon. Res. **7**, 1051–1060 (2019).
28. A. Basiri, X. Chen, J. Bai, P. Amrollahi, J. Carpenter, Z. Holman, C. Wang, and Y. Yao, "Nature-inspired chiral metasurfaces for circular polarization detection and full-Stokes polarimetric measurements," Light Sci. Appl. **8**, 78 (2019).
29. A. Arbabi, Y. Horie, M. Bagheri, and A. Faraon, "Dielectric metasurfaces for complete control of phase and polarization with subwavelength spatial resolution and high transmission," Nat. Nanotechnol. **10**, 937–943 (2015).
30. E. Arbabi, S. M. Kamali, A. Arbabi, and A. Faraon, "Full-Stokes imaging polarimetry using dielectric metasurfaces," ACS Photon. **5**, 3132–3140 (2018).
31. C. Yan, X. Li, M. Pu, X. Ma, F. Zhang, P. Gao, K. Liu, and X. Luo, "Midinfrared real-time polarization imaging with all-dielectric metasurfaces," Appl. Phys. Lett. **114**, 161904 (2019).
32. J. Hu, X. Zhao, Y. Lin, A. Zhu, X. Zhu, P. Guo, B. Cao, and C. Wang, "All-dielectric metasurface circular dichroism waveplate," Sci. Rep. **7**, 41893 (2017).
33. M. M. Rahman, A. Khaleque, M. T. Rahman, and F. Rabbi, "Gold-coated photonic crystal fiber based polarization filter for dual communication windows," Opt. Commun. **461**, 125293 (2020).
34. M. V. Gorkunov, V. E. Dmitrienko, A. A. Ezhov, V. V. Artemov, and O. Y. Rogovet, "Implications of the causality principle for ultra chiral metamaterials," Sci. Rep. **5**, 9273 (2015).
35. E. D. Palik, *Handbook of Optical Constants of Solids* (Academic, 1997).
36. S. Chou and W. Deng, "Subwavelength amorphous silicon transmission gratings and applications in polarizers and waveplates," Appl. Phys. Lett. **67**, 742–744 (1995).
37. Z. Zhang, F. Dong, T. Cheng, K. Qiu, Q. Zhang, W. Chu, and X. Wu, "Nano-fabricated pixelated micropolarizer array for visible imaging polarimetry," Rev. Sci. Instrum. **85**, 105002 (2014).